LBL-21734
c.2

Lawrence Berkeley Laboratory
UNIVERSITY OF CALIFORNIA

RECEIVED
LAWRENCE
BERKELEY LABORATORY

AUG 12 1986

LIBRARY AND
DOCUMENTS SECTION

Materials & Molecular Research Division

THE MERCUROUS DI-ION (Hg_2^{+2}), A THEORETICAL STUDY

R.P. Neisler
(Ph.D. Thesis)

June 1986

TWO-WEEK LOAN COPY
This is a Library Circulating Copy
which may be borrowed for two weeks.

Prepared for the U.S. Department of Energy under Contract DE-AC03-76SF00098

LBL-21734
c.2

DISCLAIMER

This document was prepared as an account of work sponsored by the United States Government. While this document is believed to contain correct information, neither the United States Government nor any agency thereof, nor the Regents of the University of California, nor any of their employees, makes any warranty, express or implied, or assumes any legal responsibility for the accuracy, completeness, or usefulness of any information, apparatus, product, or process disclosed, or represents that its use would not infringe privately owned rights. Reference herein to any specific commercial product, process, or service by its trade name, trademark, manufacturer, or otherwise, does not necessarily constitute or imply its endorsement, recommendation, or favoring by the United States Government or any agency thereof, or the Regents of the University of California. The views and opinions of authors expressed herein do not necessarily state or reflect those of the United States Government or any agency thereof or the Regents of the University of California.

The Mercurous Di-Ion (Hg_2^{+2}), A Theoretical Study

Randy Paul Neisler
Ph.D. Thesis

Lawrence Berkeley Laboratory
University of California
Berkeley, California 94720

This work was supported by the Director, Office of Energy Research, Office of Basic Energy Sciences, Chemical Sciences Division of the U.S. Department of Energy under Contract Number DE-AC03-76SF00098.

The Mercurous Di-Ion (Hg_2^{+2}), A Theoretical Study

Randy P. Neisler

Abstract

Electronic structure calculations are performed on the ground state of the mercurous di-ion, Hg_2^{+2}, using relativistic effective core potentials. In addition, a parallel calculation is carried out on a non-relativistic basis where the speed of light is assigned a value of $c = 10^5$ a.u. Equilibrium bond distances, R_e, and dissociation energies, D_e, are calculated at the self-consistent field (SCF) level using spin-averaged effective potentials and at the configuration interaction (CI) level, which includes spin-orbit terms. The CI bond distances and dissociation energies are 2.539 Å and -26.3 kcal/mole, relativistically, and 2.819 Å and -49.6 kcal/mole, non-relativistically. These results are compared with previous values from a Hartree-Fock-Slater calculation. Similarities with isoelectronic gold dimer, Au_2, are also discussed.

The mercurous di-ion is metastable in the gas phase but is stable in aqueous solution. A continuum dielectric method is used to approximate the free energy, enthalpy, and entropy of hydration of the system. The ion is placed within a dielectric cavity of predetermined shape with various constraints used to determine the cavity size. Results are analyzed in terms of reaction enthalpies with comparisons made to experimental values.

TABLE OF CONTENTS

Chapter Page

List of Figures.....iii

List of Tables.....iv

1. Introduction.....1

2. Electronic structure calculations of the mercurous di-ion.....2

2.1 Background.....2

2.2 Effective core potentials from atomic DHF calculations....4

2.2.1 The DHF approximation.....4

2.2.2 Results of DHF calculation.....7

2.2.3 Pseudo orbitals.....9

2.2.4 Effective potentials.....10

2.2.5 Spin-orbit operator.....13

2.3 SCF calculations.....14

2.3.1 Basis set.....14

2.3.2 SCF results for mercurous ion.....16

2.3.3 SCF results for the di-ion.....16

2.4 CI calculations.....20

3. Electrostatic models of solvation.....30

3.1 Background.....30

3.2 Cavity approximations.....32

3.2.1 Sphere.....32

3.2.2 Prolate spheroid.....37

3.2.3 Correction to prolate spheroid.....42

3.3 Cavity radii and free energies.....44

3.4 Solvation entropies and enthalpies.....49

4. Solvation of the mercurous di-ion.....53

4.1 Enthalpies from internal energies.....53

4.2 Modified energy curves and experimental results.....58

References.....64

LIST OF FIGURES

Figure	Page
2.1	21
4.1	60

LIST OF TABLES

Table	Page
2.1	8
2.2	11
2.3	15
2.4	17
2.5	18
2.6	23
2.7	24
2.8	27
3.1	46
3.2	47
3.3	48
3.4	51
3.5	52
4.1	57
4.2	59

Chapter 1

INTRODUCTION

Chemical systems involving the heavier elements reveal unusual properties. Undoubtedly, these properties can in part be attributed to the large number of electrons present. From the time of Mendeleev, surprising trends have been observed in the periodic table as the atomic number increases. In recent years, several authors have noted a correlation between these trends and the inherent relativistic effects of the systems containing the heavier elements.[1-6]

Mercury is an element of particular interest due to its surprising physical and chemical properties. Its liquid standard state and the unusual stability of many of its compounds relative to other members of its group are but a few of the traits attributed to the relativistic effects mentioned previously.[2,3] Mercurous di-ion, Hg_2^{+2}, the system considered in the following chapters of this dissertation, is a molecule of remarkable stability. Identical to gold dimer, Au_2, in electronic structure, mercurous di-ion is expected to show a similar relativistic stabilization of its bond energy as determined in the next chapter.

Although unusually stable in solution, mercurous di-ion readily dissociates as a gaseous species. Hence, in the subsequent chapters a model is developed to determine the stabilization due to solvation effects, which are then used to modify the gaseous internal energy curves.

Chapter 2

ELECTRONIC STRUCTURE CALCULATIONS OF THE MERCUROUS DI-ION

2.1 BACKGROUND

It has long been realized that the majority of chemical and physical properties of atomic and molecular systems are dominated by valence electron interactions with the core electrons providing shielding effects and an effective field. A method that requires only the valence electrons to be considered while representing the core with an effective potential is most desirable given the high computer costs of all-electron calculations involving atoms with many electrons.

Historically, the concept of treating an electron as a subset of the other electrons present originated with the work of Fock, Vesselow, and Petraschen.[7] The use of effective potentials received theoretical justification in 1959 from Phillips and Kleinman[8] and was extended to many valence electrons by Weeks and Rice.[9]

A variety of methods are now used to generate effective potentials and are described in the review by Krauss and Stevens.[10] Our method,[6,11-21] outlined more fully in the following sections, involves forming pseudo orbitals using relativistic Dirac-Fock orbitals and then inverting the one-electron equation[11]

$$(-\tfrac{1}{2}\nabla^2 - Z/r + U_v^{REP} + W_v)\chi_v = \varepsilon_v \chi_v \qquad (2.1)$$

where U_v^{REP} is the effective potential, χ_v is the pseudo orbital, and ε_v is the Dirac-Fock orbital energy. Furthermore, W_v includes the coulomb and exchange terms from the interaction of the electron in orbital v

with all the other electrons in the valence region. The reliability of computations using potentials generated in this manner in comparison to all-electron calculations is well documented,[10] yielding results with agreement often to within a few percent.

As previously stated, effective potentials can be found once the Dirac-Fock orbitals are determined. The next section describes the procedure used in finding these orbitals.

2.2 EFFECTIVE CORE POTENTIALS FROM ATOMIC DHF CALCULATIONS

2.2.1 The DHF approximation

The Dirac-Fock method[22,25-27] involves the solution of the energy equation with the relativistic Hamiltonian for n electrons given by

$$H^{rel} = \sum_{i=1}^{n} (c\alpha.p_i + m\beta c^2 - Ze^2/r_i) + \sum_{i>j} e^2/r_{ij} \qquad (2.2)$$

where the exchange corrections approximated by the Breit interaction terms are neglected. The terms in equation (2.2) are as follows; r_i is the distance of electron i from the nucleus of charge Z, α_i is a vector whose components are 4x4 matricies

$$\alpha_x = \begin{vmatrix} 0 & 0 & 0 & 1 \\ 0 & 0 & 1 & 0 \\ 0 & 1 & 0 & 0 \\ 1 & 0 & 0 & 0 \end{vmatrix}, \quad \alpha_y = \begin{vmatrix} 0 & 0 & 0 & -i \\ 0 & 0 & i & 0 \\ 0 & -i & 0 & 0 \\ i & 0 & 0 & 0 \end{vmatrix}, \quad \alpha_z = \begin{vmatrix} 0 & 0 & 1 & 0 \\ 0 & 0 & 0 & -1 \\ 1 & 0 & 0 & 0 \\ 0 & -1 & 0 & 0 \end{vmatrix}$$

$$\beta = \begin{vmatrix} 1 & 0 & 0 & 0 \\ 0 & 1 & 0 & 0 \\ 0 & 0 & -1 & 0 \\ 0 & 0 & 0 & -1 \end{vmatrix}, \quad \text{and} \quad p_i = -ih\nabla_i.$$

The eigenfunctions for the Hamiltonian in equation (2.2) are four component Dirac spinors

$$\Psi_{n\kappa m} = \begin{vmatrix} P_{n\kappa}(r)/r & \chi_{\kappa m}(\theta,\phi) \\ iQ_{n\kappa}(r)/r & \chi_{-\kappa m}(\theta,\phi) \end{vmatrix} \qquad (2.3)$$

with $P_{n\kappa}(r)$ and $Q_{n\kappa}(r)$ defined as the large and small radial components, respectively. The angular portion is expressed as

$$\chi_{\kappa m}(\theta,\phi) = \sum_{\sigma=\pm 1/2} C(\ell\, 1/2\, j; m-\sigma,\sigma)\, Y_{\lambda}^{m-\sigma}(\theta,\phi)\, \Phi_{1/2}^{\sigma} \qquad (2.4)$$

where $C(\ell\, 1/2\, j; m-\sigma, \sigma)$ are Clebsch-Gordan coefficients, $Y_\lambda^{m-\sigma}(\theta,\phi)$ is a spherical harmonic and $\phi^{q}_{1/2}$ are Pauli spinors. The quantum number kappa is defined as $\kappa = \ell$ if $j = \ell - 1/2$ and $\kappa = -(\ell+1)$ if $j = \ell + 1/2$. Furthermore, the index λ is $\lambda = |y + 1/2| - 1/2$ where y is either κ or $-\kappa$ as indicated in equation (2.3).

For a given value of kappa the radial components $P_{n\kappa}(r)$ and $Q_{n\kappa}(r)$ form an orthonormal set,

$$\int_0^\infty [\, P_{n'\kappa}(r)\, P_{n\kappa}(r) + Q_{n'\kappa}(r)\, Q_{n\kappa}(r)\,]\, dr = \delta_{n'n} \qquad (2.5)$$

and, furthermore, they satisfy the following coupled differential equations

$$dP_{n\kappa}(r)/dr + \kappa P_{n\kappa}(r)/r - \{2/\alpha + \alpha(V_i(r) - \varepsilon_{n\kappa})\} Q_{n\kappa}(r) = X_Q(r) \qquad (2.6)$$

$$dQ_{n\kappa}(r)/dr - \kappa Q_{n\kappa}(r)/r + \alpha\{V_i(r) - \varepsilon_{n\kappa}\} P_{n\kappa}(r) = X_P(r) \qquad (2.7)$$

where $V_i(r)$ and $X_{P,Q}(r)$ are the coulomb potential and exchange terms, respectively, $\alpha = 1/c$ is the fine structure constant, and $\varepsilon_{n\kappa}$ is the one-electron energy.

Computer codes developed by Desclaux[23,24] and based upon the foundational work of Grant[25-27] are used to solve the two first order coupled differential equations, in which a change of variable is made with $t = \ln r$. The resultant equations are then

$$dP/dt + \kappa P - \{\, 2r/\alpha + \alpha r(V_i(r) - \varepsilon_{n\kappa})\} Q = rX_Q \qquad (2.8)$$

$$dQ/dt - \kappa Q + \alpha r\{\, V_i(r) - \varepsilon_{n\kappa}\} P = rX_P. \qquad (2.9)$$

These are solved using the five point Adams predictor-corrector method[28] where

$$p_{n+1} = y_n + \frac{h}{720}\,(1901y'_n - 2774y'_{n-1} + 2616y'_{n-2} - 1274y'_{n-3} + 251y'_{n-4}) \qquad (2.10)$$

$$c_{n+1} = y_n + \frac{h}{720}\,(251p'_{n+1} + 646y'_n - 264y'_{n-1} + 106y'_{n-2} - 19y'_{n-3}) \qquad (2.11)$$

$$y_{n+1} = \frac{1}{502}\,(475c_{n+1} + 27p_{n+1}) \qquad (2.12)$$

are the predictor, corrector, and the resultant value. The y_n term denotes the solution at the nth iteration. Furthermore, the prime implies differentiation and h is a constant interval.

The integration is performed both from the origin outward and from practical infinity inward. The outward integration begins from a power series expansion with a point charge nucleus and the inward starts from the asymptotic form $P(r) = p\exp(-\mu r)$, $Q(r) = q\exp(-\mu r)$ with $\mu = (\varepsilon - \varepsilon^2/4c^2)^{1/2}$ and $\mu p = (2c - \varepsilon/2c)q$. The energy eigenvalue ε is then varied until the inward and outward integrations give the same value for the large component at the match point. In general, two different values will exist for the small radial component, Q_{inner} and Q_{outer}, unless ε has been chosen correctly. A functional integration of ε provides a corrected value and the integration processs is repeated until convergence is achieved.

The Dirac-Fock calculation is performed, first, in a fully relativistic manner and, again, in the non-relativistic limit. The non-relativistic calculation involves assigning a large enough value to the speed of light, in our case $c = 10^5$ a.u., such that the small radial

components approach zero and the large radial components approach the non-relativistic Hartree-Fock values.

2.2.2 Results of DHF calculation

The $^2S_{1/2}$ ground state and six excited states are determined for the mercurous ion. Excited state orbitals are obtained by promoting the lone 6s electron to an excited orbital while the remaining electrons maintain their ground state wave functions. The valence electron configurations of the mercurous ion considered are $5d^{10}6s$, $5d^{10}6p^*$, $5d^{10}6p$, $5d^{10}5f^*$, $5d^{10}5f$, $5d^{10}5g^*$, and $5d^{10}5g$, where the * represents the orbital with the lower j value. The one-electron energies obtained from the DHF calculation, both relativistic and non-relativistic, along with their corresponding R_{max} values for the large radial component are listed in table 2.1.

From table 2.1 it is apparent that electrons of low angular momentum have lower relativistic orbital energies as compared to those obtained in the non-relativistic limit. Similarly, those with high angular momentum have higher orbital energies. In fact, the relativistic shift in energy is great enough to change the ordering of some orbitals as seen in the 5s and 4f,4f* values, where the 5s orbital is now lower in energy than the two 4f orbitals. A similar trend is seen in a comparison of R_{max} values for the large radial components. The electrons of low(high) angular momentum exhibit a contraction(expansion) of the large radial component in the relativistic case as compared to the non-relativistic.

Another important relativistic effect, the spin orbit splitting, can be obtained from the orbital energies of table 2.1. In the valence

Table 2.1:

Hg^+ orbital energies and R_{max} values are obtained from DHF calculations(a.u.). The orbitals 1s-6s are from the (core)$5d^{10}6s^1$ ground state configuration, whereas the 6p*-5g orbitals are from excited states in which only the lone 6s electron is promoted to higher electronic states while the remaining orbitals maintain their ground state configurations (see text).

ORBITAL	REL(-ε)	NREL(-ε)	REL Rmax	NREL Rmax
1s	3.0765e 03	2.7790e 03	1.0226e-02	1.2257e-02
2s	5.5086e 02	4.7103e 02	5.9355e-02	6.8266e-02
2p*	5.2718e 02	4.5247e 02	4.3711e-02	5.2983e-02
2p	4.5547e 02	4.5247e 02	5.1165e-02	5.2983e-02
3s	1.3350e 02	1.1343e 02	1.6698e-01	1.8622e-01
3p*	1.2296e 02	1.0463e 02	1.5589e-01	1.7530e-01
3p	1.0687e 02	1.0463e 02	1.7090e-01	1.7530e-01
3d*	8.9758e 01	8.8436e 01	1.3318e-01	1.3772e-01
3d	8.6342e 01	8.8436e 01	1.3738e-01	1.3772e-01
4s	3.0988e 01	2.5864e 01	3.7667e-01	4.1450e-01
4p*	2.6449e 01	2.1990e 01	3.7530e-01	4.1394e-01
4p	2.2512e 01	2.1990e 01	4.0515e-01	4.1394e-01
4d*	1.5121e 01	1.4901e 01	3.9813e-01	4.0648e-01
4d	1.4377e 01	1.4901e 01	4.0780e-01	4.0648e-01
4f*	4.7970e 00	5.3036e 00	3.6606e-01	3.6309e-01
4f	4.6358e 00	5.3036e 00	3.7089e-01	3.6309e-01
5s	5.4297e 00	4.4721e 00	8.3653e-01	9.2078e-01
5p*	3.8655e 00	3.1438e 00	8.8214e-01	9.7402e-01
5p	3.1704e 00	3.1438e 00	9.5745e-01	9.7402e-01
5d*	9.7539e-01	1.0056e 00	1.1370e 00	1.1491e 00
5d	8.9965e-01	1.0055e 00	1.1764e 00	1.1491e 00
6s	6.3924e-01	5.3500e-01	2.2248e 00	2.5550e 00
6p*	4.1858e-01	3.6935e-01	2.7813e 00	3.1577e 00
6p	3.8141e-01	3.6935e-01	3.0945e 00	3.1577e 00
5f*	1.2598e-01	1.2591e-01	7.8743e 00	7.9624e 00
5f	1.2607e-01	1.2591e-01	7.8616e 00	7.9624e 00
5g*	8.0010e-02	8.0006e-02	1.2505e 01	1.2506e 01
5g	8.0010e-02	8.0006e-02	1.2505e 01	1.2506e 01

region, only the 5d*,5d and 6p*,6p orbitals have significant splittings equivalent to 2.0610 and 1.0115 ev for each orbital pair, respectively. The 5f*,5f and 5g*,5g orbital pairs have negligibly small splittings since they are very loosely bound.

2.2.3 Pseudo orbitals

Of the various methods used in generating pseudo orbitals[10,15,29-32] we use the procedure developed by Christiansen[15] in which shape consistent orbitals are formed where the pseudo orbitals are identical to the Dirac-Fock orbitals beyond a prescribed match point. In this method, the dominant criterion in forming pseudo orbitals is that the W_v in equation (2.1) should be the same regardless of whether the true orbitals or pseudo orbitals are used. Although slight differences in W_v are unavoidable when using pseudo orbitals, these differences are judged unimportant[15] if confined to a small region about the nucleus whereas exact equality with the true orbital at large r is essential. The differences in W_v for small r are only that which are necessary to satisfy the criteria of a normalized, smooth, and nodeless orbital.

The pseudo orbitals are formed using only the large component of the Dirac-Fock wavefunction since the effect of the small component is negligible in the valence region.[11] This methodology is necessary since nodes cannot be removed simultaneously from both the large and small components.

The pseudo orbitals are defined in two sections. The first section extends from infinity to some match point, R_{match}, and is equivalent to the large radial component from the DHF calculation. The other section

extends from R_{match} to the origin and is expressed as a five term polynomial in r with a lead power, typically, of $\ell + 2$.

Smoothness criteria require that the polynomial have the same value and the same first, second, and third derivatives as the outer wave function at the point R_{match}. Furthermore, it is to have no nodes and not more than two inflexions or more than three inflexions in its first derivative. Additionally, the pseudo orbital must be normalized and the value of R_{match} is to be less than R_{max}. The lead power of the polynomial expansion is reduced from $\ell + 2$, if necessary, to satisfy this criterion.

The pseudo orbitals for the mercurous ion are formed from the wavefunctions of section (2.1). The (core)$5d^{10}6s^1$ configuration is used to construct pseudo orbitals for the $s_{1/2}$, $d_{3/2}$, and $d_{5/2}$ components. In addition the six excited states are used for constructing the $p_{1/2}$, $p_{3/2}$, $f_{5/2}$, $f_{7/2}$, $g_{7/2}$, and $g_{9/2}$ pseudo orbitals. Table 2.2 contains a list of the lead powers used in the polynomial expansion and a comparison of R_{match} for the pseudo orbitals and R_{max} for the DHF large radial component. Due to the nodeless character of the 5g orbitals, the entire DHF radial function is used as the pseudo orbital, and, hence, these are not included in the table. Since the values of R_{match} are below those of R_{max}, it is clear that the dominant contribution to the pseudo orbitals is from the DHF radial component as desired.

2.2.4 Effective potentials

From the pseudo orbitals, effective potentials are obtained which satisfy the one electron equation[11,29]

Table 2.2:

R_{match} vs R_{max} values for Hg^+ valence orbitals(a.u.), where N is the lead power in the polynomial expansion of pseudo orbital.

ORBITAL	N	REL Rmatch	REL Rmax	NREL Rmatch	NREL Rmax
5d*	4	1.0648e 00	1.1370e 00	1.0648e 00	1.1491e 00
5d	4	1.1194e 00	1.1764e 00	1.0648e 00	1.1491e 00
6s	2	2.0397e 00	2.2248e 00	2.2542e 00	2.5550e 00
6p*	3	2.2542e 00	2.7813e 00	2.4913e 00	3.1577e 00
6p	3	2.4913e 00	3.0945e 00	2.4913e 00	3.1577e 00
5f*	3	6.1276e 00	7.8743e 00	6.1276e 00	7.9624e 00
5f	3	6.1276e 00	7.8616e 00	6.1276e 00	7.9624e 00

$$(-\tfrac{1}{2}\nabla^2 - Z/r + U_v^{REP} + W_v)\chi_v = \varepsilon_v \chi_v \tag{2.13}$$

which is described on page 2.

Equation (2.13) can be solved for U_v^{REP} provided χ_v is nodeless, hence,

$$U_v^{REP} = [(\varepsilon_v + \tfrac{1}{2}\nabla^2 + Z/r - W_v)\chi_v]/\chi_v. \tag{2.14}$$

Furthermore, the overall potential for an atom involves sums over ℓ, j, and m

$$U^{REP} = \sum_{\ell=0}^{\infty} \sum_{j=|\ell-1/2|}^{\ell+1/2} \sum_{m=-j}^{j} U_{\ell j}^{REP} |\ell j m\rangle\langle \ell j m| \tag{2.15}$$

where the projection operators are two component spinors equivalent to the angular factors of the two large components of the Dirac spinors. In principle the sum over ℓ is from zero to infinity, however, it has been shown[11] that $U_{\ell j}^{REP}$ does not change appreciably after ℓ exceeds by one the highest value of ℓ in the core. The expression for U^{REP} is now

$$U^{REP} = U_{LJ}^{REP} + \sum_{\ell=0}^{L} \sum_{j=|\ell-1/2|}^{\ell+1/2} \sum_{m=-j}^{j} [U_{\ell j}^{REP} - U_{LJ}^{REP}] \, |\ell j m\rangle\langle \ell j m|. \tag{2.16}$$

However, for use in standard molecular SCF programs based on A-S coupling[12], the potentials are spin-averaged according to the expression

$$U_\ell^{AREP} = (2\ell+1)^{-1}[(\ell+1)\, U_{\ell,\ell+1/2}^{REP} + \ell\, U_{\ell,\ell-1/2}^{REP}]. \tag{2.17}$$

This averaging is advantageous since, considering the relativistic

effects contained in the effective potentials, only the spin-orbit effect is eliminated in the process but is eventually recovered in the CI calculation. The overall potential is now written as

$$U^{AREP} = U_L^{AREP} + \sum_{\ell=0}^{L} \sum_{m=-\ell}^{\ell} [\, U_\ell^{AREP} - U_L^{AREP}]\, |\ell m\rangle\langle \ell m| \qquad (2.18)$$

which compared with equation (2.16) is no longer j dependent.

2.2.5 Spin-orbit operator

Spin-orbit effects are re-introduced at the CI level by use of a spin-orbit operator[19] defined as the difference of the U^{REP} and U^{AREP},

$$H^{SO} = U^{REP} - U^{AREP}$$

$$= \sum_{\ell=1}^{L-1} (U^{REP}_{\ell,\ell+1/2}(r) - U^{REP}_{\ell,\ell-1/2}(r))$$

$$\times [\, \frac{\ell}{2\ell+1} \sum_{-\ell-1/2}^{\ell+1/2} |\ell,\ell+1/2,m\rangle\langle \ell,\ell+1/2,m|$$

$$- \frac{\ell+1}{2\ell+1} \sum_{-\ell+1/2}^{\ell-1/2} |\ell,\ell-1/2,m\rangle\langle \ell,\ell-1/2,m|\,] \qquad (2.19)$$

where the difference $U_{LJ}^{REP}(r) - U_L^{AREP}(r)$ is negligible and, therefore, is not included in the operator. The spin-orbit terms are included in the CI Hamiltonian and placed on an equivalent level with the electron correlation. Since the spin-orbit matrix elements may be complex, a procedure is used which is a modification of the diagonalization routine developed by Davidson[33] made to accommodate complex elements.

2.3 SCF CALCULATIONS

It is apparent that within the averaged relativistic effective potential lie all the dominant one-electron relativistic effects, excluding spin-orbit, which influence the valence electrons, both directly and indirectly. The valence electrons can now be treated non-relativistically[11] by solving the Hartree-Fock energy equation with the inclusion of U^{AREP} in the Hamiltonian

$$H = \sum_{\mu=1}^{n_v} \{-\tfrac{1}{2}\nabla_\mu^2 + \sum_{\alpha}^{N} (-Z_\alpha/r_{\alpha\mu} + U_\alpha^{AREP})\} + \sum_{\mu<\nu} 1/r_{\mu\nu} \qquad (2.20)$$

where n_v is the number of valence electrons, and N is the number of nuclei. Z_α is defined consistently with the type of effective potential used in the calculation. For U^{AREP}, we designate Z_α to be the effective nuclear charge equal to the nuclear charge minus the number of core electrons.

2.3.1 Basis set

The valence orbitals are expressed in terms of expansions in Slater functions. The double zeta basis set in table 2.3 is derived from previously optimized functions of the mercury atom obtained from earlier preliminary calculations. The 5d and 6s zeta values are from the ground state ^1S atomic configuration, and the 6p values are from the lowest atomic ^3P state with the valence configuration $6s^1 6p^1$. The zeta's of the atomic 5d and 6s functions for the relativistic calculation are increased by 10% to account for the contraction of these orbitals with the removal of one of the 6s electrons. Additionally, the 6p functions

Table 2.3:

Hg^+ STO valence basis set

	ZETA VALUES	
	RELATIVISTIC	NON-RELATIVISTIC
$\zeta_{6s(1)}$	3.405	3.095
$\zeta_{6s(2)}$	1.975	1.796
$\zeta_{6p(1)}$	2.463	2.463
$\zeta_{6p(2)}$	1.313	1.313
$\zeta_{5d(1)}$	5.090	5.090
$\zeta_{5d(2)}$	2.705	2.705

are kept at the atomic values, since the 6p orbital contracts much less than the 5d or 6s.

As evident in table 2.1, the differences due to relativistic effects are small for the 5d and 6p orbitals as compared to the 6s. The relativistic zeta values, therefore, are used to describe the non-relativistic 5d and 6p orbitals, whereas, the atomic 6s zeta values represent the corresponding non-relativistic orbital of the ion, which, being expanded with respect to its relativistic counterpart, is more similar to the atomic orbital.

2.3.2 SCF results for mercurous ion

The reliability of the basis set can be determined by comparing the orbital energies obtained at the SCF level of a calculation on the ^2S ground state of the mercurous ion using relativistic and non-relativistic effective potentials and treating only the outer 11-electrons with those from the all electron results of section (2.1). Table 2.4 reveals good agreement between the two methods for the valence orbitals, implying that the basis set is accurately representing these orbitals in the valence region.

2.3.3 SCF results for the di-ion

The SCF molecular calculation involves a 22 electron single configuration in which the two 6s electrons are paired in a σ_g molecular orbital. The orbital coefficients near the bond distance in both the relativistic and non-relativistic cases reveal the bond to be predominantly a 6s-6s sigma bond, see table 2.5. Furthermore, the relativistic contraction of s type orbitals leads to an expectation of a

Table 2.4:

Relativistic and non-relativistic valence orbital energies(a.u.) for ^2S Hg^+ as obtained from effective potential and all-electron calculations.

	$\varepsilon_{5d_{3/2}}$	$\varepsilon_{5d_{5/2}}$	$\varepsilon_{6s_{1/2}}$
REL all e^-	0.975	0.900	0.639
REL AREP	0.947		0.636
NREL all e^-	1.01		0.535
NREL EP	1.02		0.534

Table 2.5:

SCF orbital coefficients for ground state Hg_2^{+2}.

	RELATIVISTIC		NON-RELATIVISTIC	
R(a.u.)	4.5	5.0	5.0	5.5
sσ	0.2855	0.2702	0.2620	0.2417
	0.3163	0.3472	0.3280	0.3562
pσ	0.1354	0.1203	0.1513	0.1317
	0.0202	0.0415	0.0406	0.0670
dσ	-0.1010	-0.0827	-0.0638	-0.0528
	-0.0764	-0.0577	-0.0348	-0.0247

shorter bond length in the relativistic calculation as compared to the non-relativistic. From a cubic fit of the results, equilibrium bond distances of 4.78 and 5.31 a.u. and dissociation energies relative to two dissociated mercurous ions of -0.05746 and -0.09259 hartrees are obtained for the relativistic and non-relativistic SCF calculations, respectively. The dissociation energies are negative due to the electrostatic repulsion in the system. Hence, the di-ion is metastable as a gaseous species dissociating at equilibrium to two Hg^{+}. Nevertheless, as discussed below, Hg_2^{+2} is stable in the aqueous phase where solvation effects lower the energy of the system sufficiently to provide positive dissociation energies.

2.4 CI CALCULATIONS

A CI calculation, including spin-orbit terms, is performed for the ground state of Hg_2^{+2}, involving all 10 single and 43 double excitations from the reference configuration (core)$6s\sigma_g^2$. Because of computing limitations, the number of SCF orbitals included are 6, 0, 2, 2 for σ, δ_{xy}, π_x, and π_y as opposed to a complete set of 16, 4, 8, 8. Excitations from the d-type orbitals either $\delta_{x^2-y^2}$ or δ_{xy} are excluded, not only as a result of limitations in the computing process, but also due to our assumption that the bond involves principally a 6s-6s sigma bond and the configurations involving d-type orbitals have little effect on the ground state energy.

Figure 2.1 contains the energy curves for the CI calculations with respect to the same dissociation limit as in the SCF calculation. The energy curves have vibrational frequencies of 182 cm^{-1} for the relativistic result and 115 cm^{-1} for the non-relativistic. Table 2.6 lists the equilibrium bond distances and dissociation energies for the curves of figure 2.1 as well as the results from the SCF calculations.

Table 2.7 contains the CI coefficients for the two most dominant configurations. Clearly, the configuration (core)$6s\sigma_u^2$ has a larger effect on the energy of the ground state with increasing R. As seen in table 2.6, the influence of this additional configuration causes a lengthening of the CI equilibrium bond distances with respect to the SCF results even though the di-ion is stabilized energetically. All other configurations, such as those involving the $6p_\sigma$ and $6p_\pi$ orbitals, resulting from single and double excitations out of the $6s\sigma_g^2$ orbital have CI coefficients less than 0.08, which seem to be negligible in affecting the bond energy.

Figure 2.1:

Relativistic (REL) and non-relativistic (NREL) CI energy curves for ground state mercurous di-ion, $Hg_2^{+2}(g)$, with respect to a dissociation limit of $2Hg^+(g)$ at the SCF level.

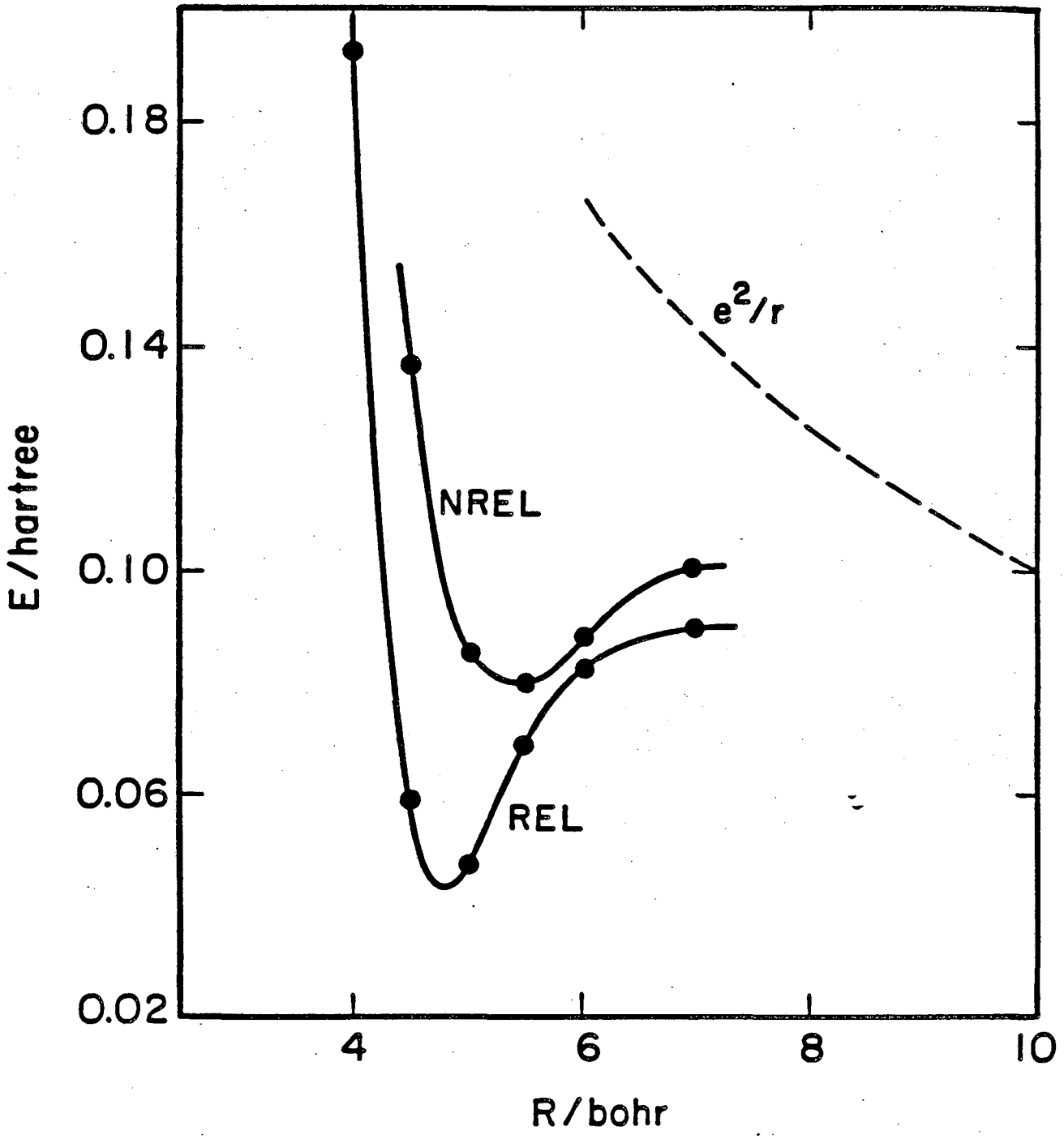
0.18
0.14
0.10
0.06
0.02
E/hartree
4
6
8
10
R/bohr
NREL
REL
e^2/r

Table 2.6:

Ground state Hg_2^{+2} SCF and CI

bond distances(R_e) and dissociation energies(D_e).

	R_e(Å)	D_e(kcal/mole)
REP SCF	2.531	-36.1
NEP SCF	2.810	-58.1
REP CI	2.539	-26.3
NEP CI	2.819	-49.6

Table 2.7:

CI coefficients for ground state Hg_2^{+2}.

	RELATIVISTIC		NON-RELATIVISTIC	
R(a.u.)	$6s\sigma_g^2$	$6s\sigma_u^2$	$6s\sigma_g^2$	$6s\sigma_u^2$
4.0	.9942	.0467		
4.5	.9924	.0681	.9918	.0431
5.0	.9884	.1089	.9900	.0599
5.5			.9887	.0866
7.0	.8908	.4372	.9574	.2469

Relativistic effects are evident in the results for Hg_2^{+2}. A relativistic contraction of the bond distance equal to 0.28 Å for both SCF and CI values is apparent. Furthermore, the bond is stabilized due to relativistic effects by 22.0 kcal/mole at the SCF level and by 23.3 kcal/mole at the CI. It has been proposed by a number of authors[2,3,5] that these effects, the contraction and stabilization of the bond, are a direct result of the relativistic effects on the valence 6s orbital, described in section (2.2.2), however, a detailed analysis is difficult as noted by Ross and Ermler.[34] Furthermore, there are others[35,36] who view the contraction and stabilization of the bond as a direct relativistic effect, unrelated to effects on the atomic orbitals.

An analysis of the accuracy of our results require comparisons either with previous calculations on Hg_2^{+2} or with results of similar molecular systems. Although there are no prior effective potential calculations on Hg_2^{+2}, results using the Hartree-Fock-Slater method are available.[35] Furthermore, the isoelectronic molecule, Au_2, is a very appropriate molecule for comparison purposes with Hg_2^{+2} since ample effective potential and all-electron calculations have been performed on this system. We first discuss the similarities with the results for Au_2 which have identical computational procedures, and then we compare our results with those from the HFS method.

As in our approach, Ross and Ermler have performed REP calculations on Au_2 involving the 10 d and single s valence electrons of the gold atom while representing the inner 68 electrons by an effective core potential. A more extensive CI calculation was involved which included single excitations from the d-type orbitals. The resulting bond distance and dissociation energy are contained in table 2.8. A non-

relativistic effective core potential calculation has been performed on Au_2 by Christiansen and Ermler.[37] Although the bond distance is an SCF result, we assume this to be sufficient for comparisons. The bond distance is also contained in table 2.8. Finally, an all-electron non-relativistic calculation by Lee et al.[13] on Au_2 is included in table 2.8 as well.

Even though there is not a non-relativistic dissociation energy value for Au_2, a comparison with Hg_2^{+2} can be undertaken in terms of the bond distance. In particular, from table 2.8, we determine a bond contraction for Au_2, in comparing REP and NEP results, equivalent to 0.36 Å versus a contraction of 0.28 Å for Hg_2^{+2}. The agreement is acceptable since, in comparing the two, we are assuming that the expansion due to the electrostatic repulsion within the Hg_2^{+2} system is balanced by the contraction resulting from the additional positive charge on each atomic core.

Nevertheless, if we remove the electrostatic repulsion from Hg_2^{+2} by subtracting the coulombic interaction energy for two positive point charges, representative of $2Hg^+$, from the configuration interaction energy of the di-ion, the resulting bond distances and dissociation energies equal to 2.46 Å and 105.7 kcal/mole, relativistically, and 2.66 Å and 71.8 kcal/mole, non-relativistically, are obtained. The agreement of the difference in the bond distance, 0.20 Å, with the difference between Au_2 REP-CI and Au_2 NREL all-electron results equivalent to 0.19 Å, is perhaps misleading, since our non-relativistic method involves effective potentials and is not an all-electron calculation. The addition of CI to the NEP calculation on Au_2, perhaps, would provide REL-NREL differences in better agreement with our results,

Table 2.8:

Hg_2^{+2} EP vs Au_2 EP, Hg_2^{+2} HFS, and Au_2 HFS

Bond distances(R_e) and dissociation energies(D_e)

	R_e(Å)	D_e(kcal/mole)
Hg_2^{+2} REP CI	2.539	- 26.3
Hg_2^{+2} NEP CI	2.819	- 49.6
Au_2 REP CI[1]	2.65	36.4
Au_2 NEP SCF[2]	3.01	
Au_2 NREL ALL e^- [3]	2.84	
Au_2 expt[1]	2.47	53.3
Hg_2^{+2} REL HFS[4]	2.63	- 11
Hg_2^{+2} NREL HFS[4]	3.12	- 46
Au_2 REL HFS[4]	2.44	58
Au_2 NREL HFS[4]	2.90	27

[1]R.B. Ross, W.C. Ermler, J.Phys. Chem. 89, 5202 (1985).

[2]P.A. Christiansen and W.C. Ermler, Mol. Phys., in press.

[3]Y.S. Lee, W.C. Ermler, K.S. Pitzer, and A.D. McLean, J. Chem. Phys., 70, 288 (1979).

[4]T. Ziegler, J.G. Snijders, and E.J. Baerends, J. Chem. Phys. 74, 1271 (1981).

although this would be contrary to what Ross and Ermler observed for the affect of CI on Au_2.[34]

However, since the computational methods are similar, we would expect an error in the results for Hg_2^{+2} of the same magnitude as obtained for Au_2 with respect to experimental values. From table 2.8, it is apparent that the calculation by Ross and Ermler overestimated the bond length in Au_2 by 0.18 Å and the dissociation energy by 16.9 kcal/mole. A similar discrepancy with experimental results is anticipated for Hg_2^{+2} as will be determined in subsequent chapters.

In table 2.8, we have also included results from an earlier relativistic calculation[35] on the mercurous di-ion. The method involves the Hartree-Fock-Slater approximation[38] where, in the one-electron energy expression, the well known Xα exchange term is included

$$V_x(\rho(r)) = -3\alpha_{ex} \left\{\frac{3}{8\pi} \rho(r)\right\}^{1/3} \tag{2.21}$$

with α_{ex}, the exchange scale factor, taken to be 0.7, and $\rho(r)$ defined as the electron density. Relativistic effects are obtained from a perturbational approach using the Pauli approximation[22] of the Dirac equation.

In comparing the two methods, it is apparent that the HFS approach yielded greater relativistic effects as seen in the differences in dissociation energies and bond distances between the relativistic and non-relativistic calculations equivalent to 35 kcal/mole and 0.49 Å for the HFS method and 23.3 kcal/mole and 0.28 Å for our results. It is difficult to say which set of results is most reliable. Additional calculations[35] reveal that the HFS method often yields inaccurate bond

distances but reasonably accurate dissociation energies compared to REP-CI calculations. Furthermore, it is possible that our non-relativistic calculation may contain some error since it is performed in the non-relativistic limit where c, the speed of light, is large but not infinite.

Nevertheless, the HFS results for Hg_2^{+2} are justified in reference (35) by a comparison with a similar HFS calculation on gold dimer, Au_2. Good agreement is claimed between the differences in bond distances and dissociation energies of the relativistic and non-relativistic calculations. However, a direct comparison between mercurous di-ion and gold dimer is difficult, as noted above, due to the inherent electrostatic repulsion of the Hg_2^{+2} system.

Furthermore, as stated previously, the HFS method tends to yield unreliable bond distances. A better comparison would be with the more reliable effective potential and all-electron calculations of table 2.8. Although our results appear to underestimate the REL-NREL difference in bond length as compared to the REP-NEP results for Au_2, the HFS method tends to overestimate this difference by (0.49 Å - 0.36Å) 0.13 Å. However, this comparison is difficult since the computational methods involved are substantially different.

A better estimation of the reliability of our result is obtained in the following chapters where we determine the hydration effects on the mercurous di-ion using a modified continuum dielectric model and obtain solvation enthalpies which can be compared with experimental results.

Chapter 3

ELECTROSTATIC MODELS OF SOLVATION

3.1 BACKGROUND

The theoretical treatment of ionic solvation has a diverse history. From the pioneering work of Max Born using a continuum electrostatic model[39] to the more recent computer simulations,[40] the topic has been of considerable interest to numerous researchers. Born's well known equation for the free energy of solvation of a spherical ion

$$\Delta G_i = -\frac{(Z_i e_o)^2}{2r_i}(1-1/\varepsilon) \qquad (3.1)$$

continues to receive some use.[41] A variety of refinements of equation (3.1) have been made involving primarily corrections to the cavity radii, r_i, and structural effects of the solvent on the ion. These are reviewed in a number of articles.[42]

Equation (3.1) and its variations involve a single rigid spherical ion. For an arbitrary charge distribution and shape, however, the result is somewhat more complicated. Kirkwood obtained expressions for the free energy of an arbitrary charge distribution in a dielectric continua for both spherical[43] and prolate spheroidal[44] cavities. The following derivations differ in the notation used from that of Kirkwood although similar results are obtained.

The electrostatic model used in determining the free energy of solvation involves placing the molecular ion within a cavity of predetermined shape which is surrounded by a dielectric continuum. The Hg_2^{+2} ion is modeled as two positive point charges placed on the z axis

at equal distances from the origin. The potentials describing the system are solutions of the Laplace equation

$$\nabla^2 \Phi = 0 \ . \tag{3.2}$$

Appropriate boundary conditions define the potential inside as well as outside the cavity assuring continuity at the cavity surface.

Given the distribution of the charges, we now consider what is the most applicable cavity shape. The most ideal would likely involve a hemispherically capped cylinder. However, numerous problems arise in determining the electrostatics of a system with this geometrical shape. Nevertheless, a close approximation to this ideal model can be obtained as is described in the following sections. The numerical results obtained from the various cavity approximations are presented in the sections following the description of the electrostatics of each system.

3.2 CAVITY APPROXIMATIONS

3.2.1 Sphere

As a preliminary calculation, a spherical cavity of radius a is considered with the electrostatic potentials expressed in spherical polar coordinates. A condition of axial symmetry as with our model yields potentials of the form[45]

$$\Phi_o = \sum_{n=0}^{\infty} (A_n r^n + B_n/r^{n+1})\, P_n(\cos\theta) \qquad r>a \tag{3.3}$$

$$\Phi_i = \sum_{n=0}^{\infty} (C_n r^n + D_n/r^{n+1})\, P_n(\cos\theta) \qquad r<a \tag{3.4}$$

where the $P_n(\cos\theta)$ are Legendre polynomials of the first kind. The coefficients A_n, B_n, C_n, and D_n are determined from the boundary conditions

$$1.\ (\Phi_o)_{r\to\infty} = 0\ ,$$

since at infinity there are no electric field sources.

$$2.\ (\Phi_o)_{r=a} = (\Phi_i)_{r=a},$$

$$3.\ \varepsilon(\partial\Phi_o/\partial r)_{r=a} = (\partial\Phi_i/\partial r)_{r=a}$$

implying that the potential and the derivative of the potential, or the normal component of the displacement vector are continuous across the boundary surface. According to the first boundary condition Φ_o remains finite as r approaches infinity, thus $A_n \equiv 0$ for every value of n.

The term $D_n/r^{n+1}\ P_n(\cos\theta)$ in the potential for $r<a$ is due to the charge distribution within the cavity equivalent to the potential in the absence of the dielectric.[45] This is derived from the law of superposition of potentials, which states that the potential due to an assembly of charges is the sum of the potentials due to each charge. Therefore, a positive point charge on the z axis a distance s from the origin, with no dielectric present, has a potential of the form[45]

$$\Phi_+ = \frac{e}{r} \sum_{n=0}^{\infty} (s/r)^n\ P_n(\cos\theta). \tag{3.5}$$

A similar expression is obtained for a positive point charge at $z=-s$

$$\Phi_- = \frac{e}{r} \sum_{n=0}^{\infty} (s/r)^n\ P_n(\cos\theta + \pi)$$

$$= \frac{e}{r} \sum_{n=0}^{\infty} (s/r)^n\ P_n(-\cos\theta). \tag{3.6}$$

The total potential is now the sum of Φ_+ and Φ_-

$$\Phi_+ + \Phi_- = \frac{e}{r} \sum_{n=0}^{\infty} (s/r)^n\ \{P_n(\cos\theta) + P_n(-\cos\theta)\}$$

$$= \frac{e}{r} \sum_{n=0}^{\infty} (s/r)^n(1+(-1)^n)\ P_n(\cos\theta) \tag{3.7}$$

and

$$D_n = es^n(1+(-1)^n). \tag{3.8}$$

The remaining coefficients are determined by applying the second and third boundary conditions

$$(\Phi_o)_{r=a} = (\Phi_i)_{r=a}$$

$$B_n/a^{n+1} = C_n a^n + es^n(1+(-1)^n)/a^{n+1} \tag{3.9}$$

and

$$\varepsilon(\partial\Phi_o/\partial r)_{r=a} = (\partial\Phi_i/\partial r)_{r=a}$$

$$-(n+1)\varepsilon B_n/a^{n+2} = nC_n a^{n-1} - es^n(1+(-1)^n)(n+1)/a^{n+2}. \tag{3.10}$$

Solved simultaneously, the above equations yield the coefficients C_n and B_n

$$C_n = \frac{es^n(1+(-1)^n)(n+1)(1-\varepsilon)}{(n+\varepsilon n+\varepsilon)\ a^{2n+1}} \tag{3.11}$$

and

$$B_n = \frac{es^n(1+(-1)^n)(2n+1)}{n+\varepsilon n+\varepsilon}. \tag{3.12}$$

The potentials Φ_o and Φ_i are now

$$\Phi_o = \sum_{n=0}^{\infty} \frac{es^n(1+(-1)^n)(2n+1)}{(n+\varepsilon n+\varepsilon)\ r^{n+1}} P_n(\cos\theta) \qquad r>a \tag{3.13}$$

$$\Phi_i = \sum_{n=0}^{\infty} \left(\frac{es^n(1+(-1)^n)(n+1)(1-\varepsilon)}{(n+\varepsilon n+\varepsilon)\ a^{2n+1}} r^n + \frac{es^n(1+(-1)^n)}{r^{n+1}}\right) P_n(\cos\theta). \qquad r<a \tag{3.14}$$

The Gibbs free energy of hydration is the mutual electrostatic energy of the interaction of the charge distribution with the surrounding dielectric. This energy is found from the reaction potential

$$\Phi_R = \sum_{n=0}^{\infty} C_n r^n P_n(\cos\theta) \tag{3.15}$$

using a charging process of the Guntelberg-Muller type,[43] and is given by one-half the sum of the products of the charge e and the value of Φ_R at the coordinates of the charges,

$$\Delta G_e = \tfrac{1}{2} \sum_{i=1}^{2} e_i \Phi_R(r_i, \theta_i, \phi_i) \tag{3.16}$$

where, for our system, the two points (r_i, θ_i, ϕ_i) are $(s,0,0)$ and $(s,\pi,0)$. The free energy is, therefore,

$$\Delta G_e = \sum_{n=0}^{\infty} \tfrac{1}{2} e\left(es^n(1+(-1)^n)(n+1)(1-\varepsilon)/(n+\varepsilon n+\varepsilon)a^{2n+1}\right)$$

$$\times\left(s^n P_n(\cos 0) + s^n P_n(\cos\pi)\right)$$

$$= \sum_{n=0}^{\infty} \tfrac{1}{2} e^2 s^{2n}(1+(-1)^n)^2(n+1)(1-\varepsilon)/(n+\varepsilon n+\varepsilon)a^{2n+1} . \tag{3.17}$$

This result is confirmed by an alternate definition of the free energy in terms of the electric field.[45] In particular, the integral,

$$\Delta G_e = -(\varepsilon-1)/8\pi \int \mathbf{E}_o \cdot \mathbf{E}_s dV, \tag{3.18}$$

is over the dielectric, only, where $\mathbf{E}_s$ is the electric field produced by the two point charges in the absence of the dielectric and is expressed as the gradient of the electrostatic potential,

$$\mathbf{E}_s = -\nabla\Phi_s = -\nabla\, D_n/r^{n+1}\, P_n(\cos\theta)$$

$$=(n+1)D_n P_n(\cos\theta)/r^{n+2}\ \mathbf{r} - D_n/r^{n+2}\partial P_n(\cos\theta)/\partial\theta\ \boldsymbol{\theta}\ . \tag{3.19}$$

Furthermore, $\mathbf{E}_o$ is the electric field in the exterior of the boundary and is expressed as

$$\mathbf{E}_o = -\nabla\Phi_o = -\nabla B_n P_n(\cos\theta)/r^{n+1}$$

$$=(n+1)B_n P_n(\cos\theta)/r^{n+2}\ \mathbf{r} - B_n/r^{n+2}\partial P_n(\cos\theta)/\partial\theta\ \breve{\boldsymbol{\theta}}. \tag{3.20}$$

These results yield the product

$$\mathbf{E}_o \cdot \mathbf{E}_s = (n+1)^2 D_n B_n P_n(\cos\theta)^2/r^{2n+4}$$

$$+ B_n D_n/r^{2n+4}\left(\partial P_n(\cos\theta)/\partial\theta\right)^2 \tag{3.21}$$

and the free energy integral

$$\Delta G_e = -\sum_{n=0}^{\infty} (\varepsilon-1)/8\pi \int_a^{\infty}\int_0^{\pi}\int_0^{2\pi} \{D_n B_n/r^{2n+4} \left((n+1)^2 P_n(\cos\theta)^2\right.$$

$$\left. + (\partial P_n(\cos\theta)/\partial\theta)^2\right)\} r^2 dr \sin\theta d\theta\, d\phi \qquad (3.22)$$

which using the relation[46]

$$\int_0^{\pi} \left(\partial P_n(\cos\theta)/\partial\theta\right)^2 \sin\theta d\theta = n(n+1) \int_0^{\pi} P_n(\cos\theta)^2 \sin\theta d\theta \qquad (3.23)$$

and the identity[46]

$$\int_0^{\pi} P_n(\cos\theta)^2 \sin\theta d\theta = 2/(2n+1) \qquad (3.24)$$

leads to the result obtained previously,

$$\Delta G_e = \sum_{n=0}^{\infty} \tfrac{1}{2} e^2 s^{2n} (1+(-1)^n)^2 (n+1)(1-\varepsilon)/(n+\varepsilon n+\varepsilon) a^{2n+1} \ . \qquad (3.25)$$

3.2.2 Prolate spheriod

Beyond the sphere, a closer approximation to the true dielectric cavity is the prolate spheroid. A similar procedure is used in determining the free energy of hydration. The electrostatic potentials are again solutions of the Laplace equation, now expressed in prolate spheroidal coordinates, ξ,η, and ϕ which have the domains

$$1 \leq \eta \leq \infty$$

$$-1 \leq \xi \leq 1$$

$$0 \leq \phi \leq 2\pi$$

where we use the notation of reference (47). The relationship between ξ, η, and ϕ and the rectangular coordinates are as follows;

$$z = a\eta\xi \tag{3.26}$$

$$y = a\{(1-\xi^2)(\eta^2-1)\}^{1/2}\cos\phi \tag{3.27}$$

$$x = a\{(1-\xi^2)(\eta^2-1)\}^{1/2}\sin\phi \tag{3.28}$$

where the focal points of the spheroid are at $z=\pm a$, $x=y=0$.

The point charges are again at positions $z=s$ and $z=-s$ which are designated as the foci of the spheroid. If a dielectric is brought into a distance $\eta=\eta_1$, the inner and outer potentials are expressed as[47]

$$V_i = \sum_{n=0}^{\infty} \left(A_i P_n(\xi) + B_i Q_n(\xi)\right)\left(A_i' P_n(\eta) + B_i' Q_n(\eta)\right) \qquad \eta<\eta_1 \tag{3.29}$$

and

$$V_o = \sum_{n=0}^{\infty} \left(A_o P_n(\xi) + B_o Q_n(\xi)\right)\left(A_o' P_n(\eta) + B_o' Q_n(\eta)\right) \qquad \eta>\eta_1 \tag{3.30}$$

where the coefficients are determined from the boundary conditions

1. V is everywhere finite,

2. $(V_i)_{\eta=\eta_1} = (V_o)_{\eta=\eta_1}$,

3. $\varepsilon\left(\frac{\partial V_o}{\partial \eta}\right)_{\eta=\eta_1} = \left(\frac{\partial V_i}{\partial \eta}\right)_{\eta=\eta_1}$.

Using the first boundary condition, it is apparent that $B_i=B_o=0$ since

$$Q_n(\xi)_{\xi=1^+} = \infty$$

and $A_o=0$ since

$$P_n(\eta)_{\eta\to\infty} \to \infty .$$

The potentials V_i and V_o are now

$$V_i = \sum_{n=0}^{\infty} D_i P_n(\xi) P_n(\eta) + C_i P_n(\xi) Q_n(\eta) \tag{3.31}$$

$$V_o = \sum_{n=0}^{\infty} C_o P_n(\xi) Q_n(\eta). \tag{3.32}$$

The term $C_i P_n(\xi) Q_n(\eta)$, analogous to the expression $D_n/r^{n+1}\ P_n(\cos\theta)$ in the spherical cavity, is due to the charge distribution within the cavity equivalent to the potential without the dielectric. As before, using the law of the superposition of potenitals, we obtain the total potential is the sum of the potentials of the two ions. The potential of a point charge at coordinates (η_o,ξ_o) is[47]

$$V_+ = \sum_{n=0}^{\infty} \frac{e}{a} (2n+1)\ P_n(\xi_o)P_n(\eta_o)P_n(\xi)Q_n(\eta). \tag{3.33}$$

Similarly, from the charge at coordinates $(\eta_o,-\xi_o)$, the potential is

$$V_- = \sum_{n=0}^{\infty} \frac{e}{a} (2n+1)(-1)^n P_n(\xi_o)P_n(\eta_o)P_n(\xi)Q_n(\eta). \tag{3.34}$$

The coefficient C_i is ,therefore,

$$C_i = \frac{e}{a}(2n+1)(1+(-1)^n)\ P_n(\xi_o)P_n(\eta_o)\ . \tag{3.35}$$

The second and third boundary conditions yield the equations

$$(V_i)_{\eta=\eta_1} = (V_o)_{\eta=\eta_1}$$

$$D_i P_n(\eta_1)+C_i Q_n(\eta_1) = C_o Q_n(\eta_1) \tag{3.36}$$

and

$$\varepsilon\left(\frac{\partial V_o}{\partial \eta}\right)_{\eta=\eta_1} = \left(\frac{\partial V_i}{\partial \eta}\right)_{\eta=\eta_1}$$

$$D_i P_n'(\eta_1) + C_i Q_n'(\eta_1) = \varepsilon C_o Q_n'(\eta_1) \tag{3.37}$$

where the prime denotes differentiation with respect to the argument. The coefficients are determined by solving the above two equations simultaneously for C_o and D_i in terms of C_i

$$C_o = \frac{C_i\left(Q_n'(\eta_1) - Q_n(\eta_1)P_n'(\eta_1)/P_n(\eta_1)\right)}{\varepsilon Q_n'(\eta_1) - Q_n(\eta_1)P_n'(\eta_1)/P_n(\eta_1)} \tag{3.38}$$

and

$$D_i = C_i\left(\frac{Q_n'(\eta_1)-Q_n(\eta_1)P_n'(\eta_1)/P_n(\eta_1)}{\varepsilon Q_n'(\eta_1)-Q_n(\eta_1)P_n'(\eta_1)/P_n(\eta_1)} -1\right) \frac{Q_n(\eta_1)}{P_n(\eta_1)} \ . \tag{3.39}$$

As with the sphere, the reaction potential can be derived from the inner electrostatic potential and is equivalent to

$$V_R = \sum_{n=0}^{\infty} D_i P_n(\xi) P_n(\eta) \ . \tag{3.40}$$

Furthermore, the free energy is again the sum of equation (3.16) with $\Phi_R(r_i,\theta_i,\phi_i)$ replaced by $V_R(\xi_i,\eta_i,\phi_i)$

$$\Delta G_e = \tfrac{1}{2}\sum_{i=1}^{2} e_i V_R(\xi_i,\eta_i,\phi_i) \ . \tag{3.41}$$

The reaction potential is evaluated at the two points (ξ_i,η_i,ϕ_i) equivalent to $(\xi_0,\eta_0,0)$ and $(-\xi_0,\eta_0,0)$, yielding the free energy

$$\begin{aligned}\Delta G_e = \sum_{n=0}^{\infty} \tfrac{1}{2} e\Big[\tfrac{e}{a}(2n+1)(1+(-1)^n)P_n(\xi_0)P_n(\eta_0)\,\frac{Q_n(\eta_1)}{P_n(\eta_1)} \\ \times \left(\frac{Q_n'(\eta_1)-Q_n(\eta_1)P_n'(\eta_1)/P_n(\eta_1)}{\varepsilon Q_n'(\eta_1)-Q_n(\eta_1)P_n'(\eta_1)/P_n(\eta_1)} -1\right) \\ \times \left(P_n(\xi_0)P_n(\eta_0)+(-1)^n P_n(\xi_0)P_n(\eta_0)\right)\end{aligned}$$

$$\begin{aligned}= \sum_{n=0}^{\infty} \tfrac{1}{2}\frac{e^2}{a}(2n+1)(1+(-1)^n)^2 P_n(\xi_0)^2 P_n(\eta_0)^2\,\frac{Q_n(\eta_1)}{P_n(\eta_1)} \\ \times \left(\frac{Q_n'(\eta_1)-Q_n(\eta_1)P_n'(\eta_1)/P_n(\eta_1)}{\varepsilon Q_n'(\eta_1)-Q_n(\eta_1)P_n'(\eta_1)/P_n(\eta_1)} -1\right) \ ,\end{aligned} \tag{3.42}$$

where $(\xi_o,\eta_o)=(1,1)$ since the point charges are at the foci of the spheroid. This result can also be confirmed by the alternate definition of the free energy equation (3.18) as discussed previously.

3.2.3 Correction to prolate spheroid

A final approximation to the ideal hemispherically capped cylinder model can be obtained by the addition of a correction term to the free energy of the prolate spheroidal cavity. The correction term amounts to effectively trimming the middle of the spheroid to a cylindrical shape while allowing the ends to retain their spheroidal surface.

The correction is derived from equation (3.18) for the free energy. The integral is approximated by evaluating the product $E_o \cdot E_s$ at the point $(\xi,\eta,\phi)=(0,\eta_1,0)$ and then evaluating the remaining volume integral. As with the sphere, the fields E_o and E_s are, respectively, the electric field of the charge distribution in the dielectric and the electric field without the dielectric present. Furthermore, they are now expressed as

$$E_o = -\nabla\Phi_o = -C_o\left\{\frac{\xi}{h_\xi} Q_n(\eta)P_n^{\prime}(\xi) + \frac{\eta}{h_\eta} P_n(\xi)Q_n^{\prime}(\eta)\right\} \tag{3.43}$$

and

$$E_s = -\nabla\Phi_s = -C_i\left\{\frac{\xi}{h_\xi} Q_n(\eta)P_n^{\prime}(\xi) + \frac{\eta}{h_\eta} P_n(\xi)Q_n^{\prime}(\eta)\right\} \tag{3.44}$$

where $h_\xi = a\left((\xi^2-\eta^2)/(\xi^2-1)\right)^{1/2}$ and $h_\eta = a\left((\xi^2-\eta^2)/(1-\eta^2)\right)^{1/2}$.
Evaluating the product $E_o \cdot E_s$ at the specified point $(0,\eta_1,0)$, yields the correction energy

$$\Delta G_c = \sum_{n=0}^{\infty} \frac{(1-\varepsilon)}{8\pi a^2} q^2 (2n+1)^2 (1+(-1)^n)^2$$

$$\times \left\{ \frac{Q_n'(\eta_1) - Q_n(\eta_1) P_n'(\eta_1)/P_n(\eta_1)}{\varepsilon Q_n'(\eta_1) - Q_n(\eta_1) P_n'(\eta_1)/P_n(\eta_1)} \right\}$$

$$\times \left\{ \frac{1}{a^2 \eta_1^2} Q_n(\eta_1)^2 P_n'(0)^2 + \frac{\eta_1^2 - 1}{\eta_1^2} Q_n'(\eta_1)^2 P_n(0)^2 \right\} \Delta V_d \qquad (3.45)$$

where ΔV_d is the volume of the spheroid removed, determined in the next section.

3.3 CAVITY RADII AND FREE ENERGIES

For many years it has been known that ionic cavity radii can be related to crystallographic radii.[48] In determining the size of the mercurous di-ion cavity in the above models, certain similarities exist with the mercurous fluoride crystal structure. In a recent article,[41] Rashin and Honig found that adding a correction factor of 7% to various ion-fluoride bond distances (after subtracting the fluoride radii) provided cavity radii which yielded solvation enthalpies in good agreement with experimental results. This method is extended to the mercurous di-ion by relating the distance between the ion and the point of intersection of the cavity with the z-axis to the mercurous fluoride crystal structure. This distance is expressed as[49,41]

$$R_c = 1.07\{(\text{Hg-F bond distance})-(F^- \text{radius})\}$$

$$= 1.07(2.31-0.72)\text{Å} = 1.70\text{Å}. \qquad (3.46)$$

Table 3.1 contains the cavity radii for the spherical model obtained by adding R_c to each value of s, and the resulting free energy obtained from equation (3.17).

Furthermore, the radial factor η_1 in the prolate spheroidal system is determined through the use of equation (3.26)

$$z = a\xi\eta \qquad (3.26)$$

where $\xi=1$ since the point of interest lies along the z axis.

Additionally, the foci a, as noted earlier, are equivalent to the positions of the point charges. The expression for η_1 is now

$$\eta_1 = z/a = (R_c+s)/s \ . \tag{3.47}$$

These values are listed in table 3.2 along with the resulting free energies of equation (3.42).

The correction to the free energy in section (3.2.3) involves an additional constraint to determine ΔV_d in equation (3.45). In particular, the distance from the point charge normal to the z-axis to the cavity boundary is to remain a constant equivalent to[49,41]

$$R_n = 1.07\{D - R(F^-)\}$$

$$= 1.07(2.69-0.72)\text{Å} = 2.11\text{Å} \tag{3.48}$$

where D is the perpendicular distance from the Hg-Hg axis to the fluoride ions. As is evident, the 7% correction factor is also applied to this value. Table 3.3 lists ΔV_d and the new spheroid volumes after the removal of ΔV_d, in addition to the the free energy corrections. The new free energies of the prolate spheroidal cavity after the addition of the correction term are also contained in table 3.3.

Table 3.1:

Free energy of hydration for spherical cavity.

s(Å)	a(Å)	ΔG_s(kcal/mole)
1.0584	2.7584	- 242.91
1.1907	2.8907	- 233.48
1.3230	3.0230	- 225.07
1.4553	3.1553	- 217.55
1.5876	3.2876	- 210.80
1.8522	3.5522	- 199.18

Table 3.2:

Free energy of hydration for prolate spheroidal cavity.

s(Å)	η_1	ΔG_{ps}(kcal/mole)
1.0584	2.6062	- 252.91
1.1907	2.4277	- 244.39
1.3230	2.2849	- 236.77
1.4553	2.1681	- 229.94
1.5876	2.0708	- 223.77
1.8522	1.9178	- 213.14

Table 3.3:

Volume of prolate spheroid removed (ΔV_d), corrected prolate spheroid volumes (V_{psc}), free energy correction (ΔG_{cor}) and corrected free energy for prolate spheroidal cavity (ΔG_{psc}).

s(Å)	ΔV_d(Å^3)	V_{psc}(Å^3)	ΔG_{cor}(kcal/mole)	ΔG_{psc}(kcal/mole)
1.0584	13.184	61.789	- 14.497	- 267.41
1.1907	18.022	65.993	- 17.109	- 261.50
1.3230	23.436	70.117	- 19.406	- 256.18
1.4553	29.410	74.181	- 21.434	- 251.37
1.5876	35.938	78.197	- 23.240	- 247.01
1.8522	50.586	86.120	- 26.321	- 239.46

3.4 SOLVATION ENTROPIES AND ENTHALPIES

As a matter of convenience and to avoid further approximations, we convert the free energies of the previous sections to enthalpies by use of the definition

$$\Delta H = \Delta G + T\Delta S \tag{3.49}$$

which may then be compared to experimental solvation enthalpies obtained from tabulated heats of formation. The entropy term in equation (3.49) is defined as

$$\Delta S = -\left(\frac{\partial \Delta G}{\partial T}\right) = -\left(\frac{\partial \Delta G}{\partial \varepsilon}\right)\left(\frac{\partial \varepsilon}{\partial T}\right) \tag{3.50}$$

where[50]

$$\left(\frac{\partial \varepsilon}{\partial T}\right) = -1.357\ (\varepsilon/T) \tag{3.51}$$

and $\varepsilon = 78.30$ are the values for water at 25 °C. The partial derivative $(\partial \Delta G/\partial \varepsilon)$ is expressed for the spherical cavity as

$$\left(\frac{\partial \Delta G}{\partial \varepsilon}\right) = \partial\left(\tfrac{1}{2} e^2 s^{2n}(1+(-1)^n)^2(n+1)(1-\varepsilon)/(n+\varepsilon n+\varepsilon)a^{2n+1}\right)/\partial\varepsilon$$

$$= \frac{-\tfrac{1}{2} e^2 s^{2n}(1+(-1)^n)^2(n+1)(2n+1)}{(n+\varepsilon n+\varepsilon)^2 a^{2n+1}} \tag{3.52}$$

and for the prolate spheroidal cavity as

$$\left(\frac{\partial \Delta G}{\partial \varepsilon}\right) = \partial\Big(\tfrac{1}{2}\frac{e^2}{a}(2n+1)(1+(-1)^n)^2 \frac{Q_n(\eta_1)}{P_n(\eta_1)}$$

$$\times \left(\frac{Q_{\breve{n}}'(\eta_1)-Q_n(\eta_1)P_{\breve{n}}'(\eta_1)/P_n(\eta_1)}{\varepsilon Q_{\breve{n}}'(\eta_1)-Q_n(\eta_1)P_{\breve{n}}'(\eta_1)/P_n(\eta_1)}\right)\Big)/\partial\varepsilon$$

$$= -\tfrac{1}{2}\frac{e^2}{a}(2n+1)(1+(-1)^n)^2 \frac{Q_n(\eta_1)}{P_n(\eta_1)}$$

$$\times \left(\frac{Q_{\breve{n}}'(\eta_1)^2-Q_{\breve{n}}'(\eta_1)Q_n(\eta_1)P_{\breve{n}}'(\eta_1)/P_n(\eta_1)}{(\varepsilon Q_{\breve{n}}'(\eta_1)-Q_n(\eta_1)P_{\breve{n}}'(\eta_1)/P_n(\eta_1))^2}\right). \qquad (3.53)$$

Using the values of tables 3.1 and 3.2, we obtain entropy terms for the two cavity shapes which are evaluated at T=298K. The products TΔS are listed in table 3.4 as a function of the distance s.

Solvation enthalpies are now determined using equation (3.49) and are contained in table 3.5. In determining the enthalpy for the corrected prolate spheroidal cavity, the entropy for the uncorrected prolate spheroid is used without an additional correction term since the inclusion of this term would undoubtedly not change the resulting enthalpies beyond the uncertainties from other approximations.

Table 3.4:

TΔS for spherical and prolate spheroidal cavities at 298K.

s(Å)	$T\Delta S_s$(kcal/mole)	$T\Delta S_{ps}$(kcal/mole)
1.0584	- 4.3264	- 4.4782
1.1907	- 4.1775	- 4.3373
1.3230	- 4.0477	- 4.2130
1.4553	- 3.9339	- 4.1032
1.5876	- 3.8342	- 4.0054
1.8522	- 3.6682	- 3.8406

Table 3.5:

Solvation enthalpies for spherical, prolate spheroidal, and corrected prolate spheroidal cavities.

s(Å)	ΔH_s(kcal/mole)	ΔH_{ps}(kcal/mole)	ΔH_{psc}(kcal/mole)
1.0584	- 247.24	- 257.39	- 271.89
1.1907	- 237.66	- 248.72	- 265.84
1.3230	- 229.12	- 240.99	- 260.39
1.4553	- 221.49	- 234.04	- 255.47
1.5876	- 214.64	- 227.78	- 251.02
1.8522	- 202.85	- 216.98	- 243.30

Chapter 4

SOLVATION OF THE MERCUROUS DI-ION

4.1 ENTHALPIES FROM INTERNAL ENERGIES

In our study of the mercurous di-ion thus far we have determined the internal energy of the system both relativistically and non-relativistically and have calculated solvation enthalpies using a primitive electrostatic continuum dielectric model. The internal energies at zero Kelvin of Chapter 2 may now be converted to enthalpies at 298K as follows.

To determine the enthalpy values from the internal energies for the reaction

$$2Hg^{+}(g) = Hg_2^{+2}(g), \tag{4.1}$$

first, the identity at absolute zero, $U_0 = H_0$, is applied. The enthalpy at higher temperatures is then obtained by adding to the absolute zero enthalpies corrections for the change in the internal modes of the system and a correction to account for the expansion of the gas with increased temperature. The enthalpy per mole is expressed as

$$H_{298} = H_0 + H_{tr} + H_{rot} + H_{vib} + H_{pv} \tag{4.2}$$

where

$$H_{tr} = \frac{3}{2} RT$$

is the translational correction,

$$H_{rot} = RT$$

is the rotational correction for diatomic species,

and

$$H_{pv} = RT$$

is the expansion correction. The vibrational correction is expressed as

$$H_{vib} = R\,\frac{h\nu}{k}\left(e^{h\nu/kT}-1\right)^{-1}.$$

where ν is the vibrational frequency of the molecule.

The enthalpy for the two singly charged mercurous ions, $2Hg^{+}$, at 298K is

$$H_{298,2Hg^{+}(g)} = H_{0,2Hg^{+}(g)} + 5R(298.15). \qquad (4.3)$$

For the gaseous di-ion, we obtain an enthalpy expressed as

$$H_{298,Hg_2^{+}2(g)} = H_{0,Hg_2^{+}2(g)} + \frac{7}{2}R(298.15) + H_{vib} \qquad (4.4)$$

where H_{vib} is determined for the relativistic and non-relativistic curves of figure 2.1. The relativistic energy curve has a frequency of

$$\nu = c\nu_e$$
$$= c(182\ cm^{-1}) = 5.46 \times 10^{12}\ s^{-1}$$

yielding an enthalpy correction of

$$H_{vib,rel} = R(262.10K)(e^{262.10/298.15}-1)^{-1}$$
$$= R(186.06K).$$

Additionally, for the non-relativistic energy curve with a frequency of

$$\nu = c\nu_e$$
$$= c(115\ cm^{-1}) = 3.45 \times 10^{12}\ s^{-1}$$

we obtain a vibrational enthalpy correction equal to

$$H_{vib,nrel} = R(165.56K)(e^{165.56/298.15}-1)^{-1}$$
$$= R(222.99K).$$

Furthermore, the change in enthalpy for the reaction of equation (4.1) performed relativistically is

$$\Delta H_{298}^{REL} = \Delta H_0^{REL} + \frac{7}{2} R(298.15) + R(186.06) - 5R(298.15)$$

$$= (\Delta H_0^{REL} - 0.519)\ kcal/mole. \qquad (4.5)$$

Calculated non-relativistically, the enthalpy is

$$\Delta H_{298}^{NREL} = \Delta H_0^{NREL} + \frac{7}{2} R(298.15) + R(222.99) - 5R(298.15)$$

$$= (\Delta H_0^{NREL} - 0.446) \text{ kcal/mole.} \qquad (4.6)$$

Table 4.1 contains the corresponding enthalpy values of figure 2.1 after the removal of the values of equations (4.5) and (4.6) for the respective curves.

Table 4.1:

Enthalpy values of gaseous mercurous di-ion at 298K (kcal/mole).

s(Å)	REL $\Delta H_{298,(g)}$	NREL $\Delta H_{298,(g)}$
1.0584	120.74	
1.1907	36.543	85.449
1.3230	29.704	53.623
1.4553	42.680	50.265
1.5876	51.654	54.815
1.8522	55.801	64.748

4.2 MODIFIED ENERGY CURVES AND EXPERIMENTAL RESULTS

The solvation enthalpies obtained from the three methods of Chapter 3 are now added to the results of table 4.1. New bond distances and equilibrium enthalpy values are obtained and are listed in table 4.2. These results may now be compared to the experimental heats of formation.

The enthalpy values of table 4.2 are for the reaction

$$2Hg^{+}(g) = Hg_2^{+2}(aq). \qquad \Delta H_e \quad (4.7)$$

An experimental enthalpy for this equation cannot be obtained directly from a combination of the heats of formation since the reaction involves both gaseous and aqueous ionic components, which have different reference states. Furthermore, experimental heats of formation are unavailable for either $Hg^{+}(aq)$ or $Hg_2^{+2}(g)$. Nevertheless, the enthalpy for the reaction of equation (4.7) can be determined indirectly as outlined below.

A heat of hydration is known[41] for a related mercury species, the mercuric ion Hg^{+2}. This is expressed as

$$Hg^{+2}(g) = Hg^{+2}(aq) \qquad \Delta H_1 \quad (4.8)$$

where $\Delta H_1 = -439.4$ kcal/mole. Now the enthalpy for the reaction

$$2Hg^{+}(g) = Hg(l) + Hg^{+2}(g) \qquad \Delta H_2 \quad (4.9)$$

is determined from the known heats of formation[51] as

Table 4.2:

Enthalpy values for the reaction, $2Hg^{+}(g) = Hg_2^{+2}(aq)$, using spherical(SPH), prolate spheroidal(PS), and corrected prolate spheroidal(PSC) solvation cavities.

	R_e(Å)	ΔH_e(kcal/mole)
REL SPH	2.492	-206.37
NREL SPH	2.710	-176.21
REL PS	2.496	-217.78
NREL PS	2.719	-188.26
REL PSC	2.508	-235.97
NREL PSC	2.745	-208.35

Figure 4.1:

Relativistic (REL) and non-relativistic (NREL) enthalpy values, using a corrected prolate spheroidal solvation cavity, for Hg_2^{+2}(298K,aq) as a function of the bond distance, R. Curves are with respect to a dissociation limit of $2Hg^{+}$(298K,g).

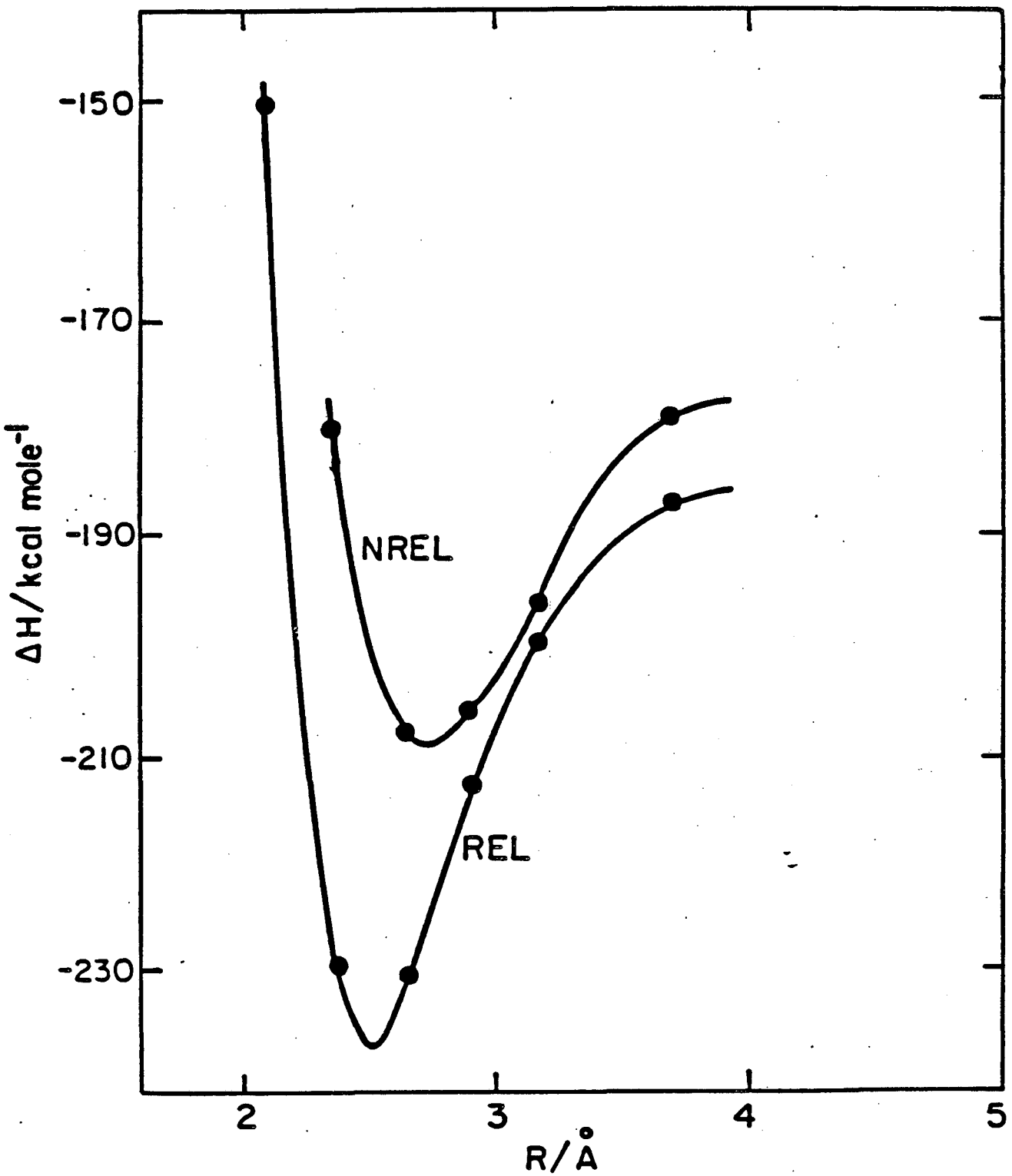
-150
-170
-190
-210
-230
ΔH/kcal mole⁻¹
NREL
REL
2
3
4
5
R/Å

$$\Delta H_2 = \Delta H_f(Hg^{+2}(g)) + \Delta H_f(Hg(l)) - 2\Delta H_f(Hg^{+}(g))$$
$$= 690.8 + 0.0 - 513.6 = 177.2 \text{ kcal/mole.}$$

Furthermore, the reaction

$$Hg(l) + Hg^{+2}(aq) = Hg_2^{+2}(aq) \qquad \Delta H_3 \quad (4.10)$$

has an enthalpy equivalent to[51]

$$\Delta H_3 = \Delta H_f(Hg_2^{+2}(aq)) - \Delta H_f(Hg^{+2}(aq)) - \Delta H_f(Hg(l))$$
$$= 41.2 - 40.9 - 0.0 = 0.3 \text{ kcal/mole.}$$

Summing the reactions of equations (4.8-4.10),

$$\begin{aligned} Hg^{+2}(g) &= Hg^{+2}(aq) && \Delta H_1 \\ + \; 2Hg^{+}(g) &= Hg(l) + Hg^{+2}(g) && \Delta H_2 \\ + \; Hg(l) + Hg^{+2}(aq) &= Hg_2^{+2}(aq) && \Delta H_3 \end{aligned}$$

and subtracting Hg(l) from each side, we obtain the desired reaction of equation (4.7)

$$2Hg^{+}(g) = Hg_2^{+2}(aq) \qquad \Delta H_4 \quad (4.11)$$

where

$$\Delta H_4 = \Delta H_1 + \Delta H_2 + \Delta H_3$$
$$= -261.9 \text{ kcal/mole.}$$

A comparison of the experimental enthalpy determined above with the results of table 4.2 reveal that the corrected prolate spheroidal solvation cavity provides the most reasonable results as anticipated. Furthermore, the discrepancy between our calculated value, -236.0 kcal/mole, and the experimental value, -261.9 kcal/mole, is well within the limitations of the calculation. This is particularly comforting since the application of an electrostatic, continuum dielectric model to systems beyond single spherical ions is uncertain at best. In fact, the greatest source of error most likely lies in the methods of Chapter 2. As noted earlier, the calculated dissociation energy for the gaseous di-ion is probably 20 kcal/mole too low since a difference of this magnitude was also determined for Au_2 using similar computational methods. In addition, the remaining 5 kcal/mole discrepancy is certainly within the uncertainties inherent in the approximations of Chapter 3.

In conclusion, it is most apparent that the application of electrostatic, continuum dielectric methods to other complex molecular systems is very promising. The reliability of the method will be determined through additional calculations and through the refinement of the procedures outlined above. Although many researchers are critical of the approach,[52] it appears that electrostatic methods will continue to be useful in understanding the theory of electrolytes.

REFERENCES

1. P. Pyykko, Adv. Quant. Chem. 11, 353 (1978).
2. P. Pyykko and J.P. Desclaux, Acc. Chem. Res. 12, 276 (1979).
3. K.S. Pitzer, Acc. Chem. Res. 12, 271 (1979).
4. P. Pyykko, ed. Proc. Symp. Relativistic Effects in Quantum Chemistry, Int. J. Quant. Chem. 25, 1 (1984).
5. G.L. Malli, ed. Relativistic Effects in Atoms, Molecules, and Solids (Plenum, New York, 1983).
6. P.A. Christiansen, W.C. Ermler, and K.S. Pitzer, Ann. Rev. Phys. Chem. 36, 407 (1985).
7. V. Fock, W. Wesselov, and M. Petraschen, Zh. Eksp. Teor. Fiz. 10, 723 (1940).
8. J.C. Phillips and L. Kleinman, Phys. Rev. 116, 287 (1959).
9. J.D. Weeks and S.A. Rice, J. Chem. Phys. 49, 2741 (1968).
10. M. Krauss and W.J. Stevens, Ann. Rev. Phys. Chem. 35, 357 (1984).
11. Y.S. Lee, W.C. Ermler, and K.S. Pitzer, J. Chem. Phys. 67, 5861 (1977).
12. W.C. Ermler, Y.S. Lee, K.S. Pitzer, and N.W. Winter, J. Chem. Phys. 69, 976 (1978).
13. Y.S. Lee, W.C. Ermler, K.S. Pitzer, and A.D. McLean, J. Chem. Phys. 70, 288 (1979).
14. W.C. Ermler, Y.S. Lee, and K.S. Pitzer, J. Chem. Phys. 70, 293 (1979).
15. P.A. Christiansen, Y.S. Lee, and K.S. Pitzer, J. Chem. Phys. 71,

4445 (1979).

16. Y.S. Lee, W.C. Ermler, and K.S. Pitzer, J. Chem. Phys. 73, 360 (1980).

17. P.A. Christiansen and K.S. Pitzer, J. Chem. Phys. 73, 5160 (1980).

18. P.A. Christiansen, K.S. Pitzer, Y.S. Lee, J.H. Yates, W.C. Ermler, and N.W. Winter, J. Chem. Phys. 75, 5410 (1981).

19. W.C. Ermler, Y.S. Lee, P.A. Christiansen, and K.S. Pitzer, Chem Phys. Lett. 81, 70 (1981).

20. P.A. Christiansen and K.S. Pitzer, Chem. Phys. Lett. 85, 434 (1981).

21. P.A. Christiansen, K. Balasubramanian, and K.S. Pitzer, J. Chem. Phys. 76, 5087 (1982).

22. H.A. Bethe and E.E. Salpeter, Quantum Mechanics of One- and Two-electron Atoms (Academic, New York, 1957).

23. J.P. Desclaux, Computer Phys. Commun. 9, 31 (1975).

24. J.P. Desclaux, D.F. Mayers, and F. O'Brien, J. Phys. B4, 631 (1971).

25. I.P. Grant, Adv. Physics 19, 747 (1970).

26. I.P. Grant, Proc. R. Soc. A 262, 555 (1961).

27. I.P. Grant, Proc. Phys. Soc. 86, 523 (1965).

28. F.B. Hildebrand, Introduction to Numerical Analysis (McGraw Hill, New York, 1956).

29. L.R. Kahn, P. Baybutt, and D.G. Truhlar, J. Chem. Phys. 65, 3826 (1976).

30. A.K. Rappe, T.A. Smedley, and W.A. Goddard III, J. Phys. Chem. 85, 1662 (1981).

31. Ph. Durand and J.C. Barthelat, Theor. Chim. Acta. 38, 283 (1975).

32. J.C. Barthelat, Ph. Durand, and A. Serafini, Mol. Phys. 33, 159 (1977).

33. E.R. Davidson, J. Comput. Phys. 17, 87 (1975).

34. R.B. Ross, W.C. Ermler, J. Phys. Chem. 89, 5202 (1985).

35. T. Ziegler, J.G. Snijders, and E.J. Baerends, J. Chem. Phys. 74, 1271 (1981).

36. W.H.E. Schwarz and S.Y. Chu, Mol. Phys. 50, 603 (1983).

37. P.A. Christiansen and W.C. Ermler, Mol. Phys., in press.

38. J.C. Slater, Phys. Rev. 81, 385 (1951).

39. M. Born, Z. Phys. 1, 45 (1920).

40. For a review, see H.C. Anderson in Modern Aspects of Electrochemistry, edited by B.E. Conway and J. O'M Brockris (Plenum, New York, 1975).

41. A.A. Rashin and B. Honig, J. Phys. Chem. 89, 5588 (1985).

42. See, for example, B.E. Conway, Ionic Hydration in Chemistry and Biophysics, (Elsevier, Amsterdam, 1981).

43. J.G. Kirkwood, J. Chem. Phys. 2, 351 (1934).

44. J.G. Kirkwood, Theory of Solutions (Gordon and Breach, New York, 1968), pp. 215-230.

45. C.F.J. Bottcher, Theory of Electric Polarization (Elsevier, Amsterdam, 1952), pp. 94-115.

46. M. Abramowitz and I.A. Stegun Handbook of Mathematical Functions (Dover, New York, 1964), p. 337.

47. W.R. Smythe, Static and Dynamic Electricity (McGraw Hill, New York, 1950), Chapter 5.

48. W.M. Latimer, K.S. Pitzer, and C.M. Slansky, J. Chem. Phys. 7, 108 (1939).

49. R.W.G. Wyckoff, Crystal Structures (Interscience, New York, 1963), Vol. 1, p. 152.

50. R.M. Noyes, J. Am. Chem. Soc. 84, 513 (1962).

51. D.D. Wagman et al., J. Phys. and Chem. Ref. Data, Vol. 11, Supp. 2.

52. D. Chandler, Ann. Rev. Phys. Chem. 29, 441 (1978).

This report was done with support from the Department of Energy. Any conclusions or opinions expressed in this report represent solely those of the author(s) and not necessarily those of The Regents of the University of California, the Lawrence Berkeley Laboratory or the Department of Energy.

Reference to a company or product name does not imply approval or recommendation of the product by the University of California or the U.S. Department of Energy to the exclusion of others that may be suitable.

LAWRENCE BERKELEY LABORATORY
TECHNICAL INFORMATION DEPARTMENT
UNIVERSITY OF CALIFORNIA
BERKELEY, CALIFORNIA 94720